

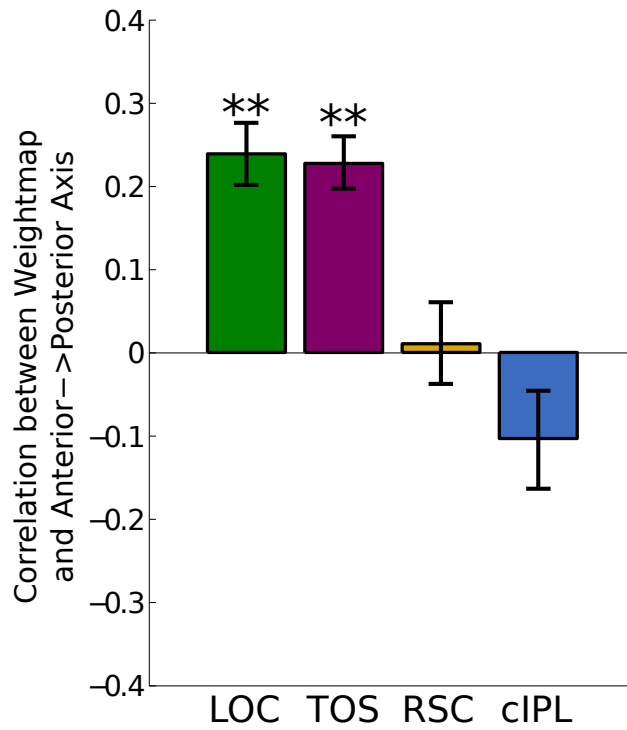
Supplementary Material for “Differential Connectivity Within the Parahippocampal Place Area”

Christopher Baldassano^{a,*}, Diane M. Beck^b, Li Fei-Fei^a

^a*Department of Computer Science, Stanford University, Stanford, CA, USA*

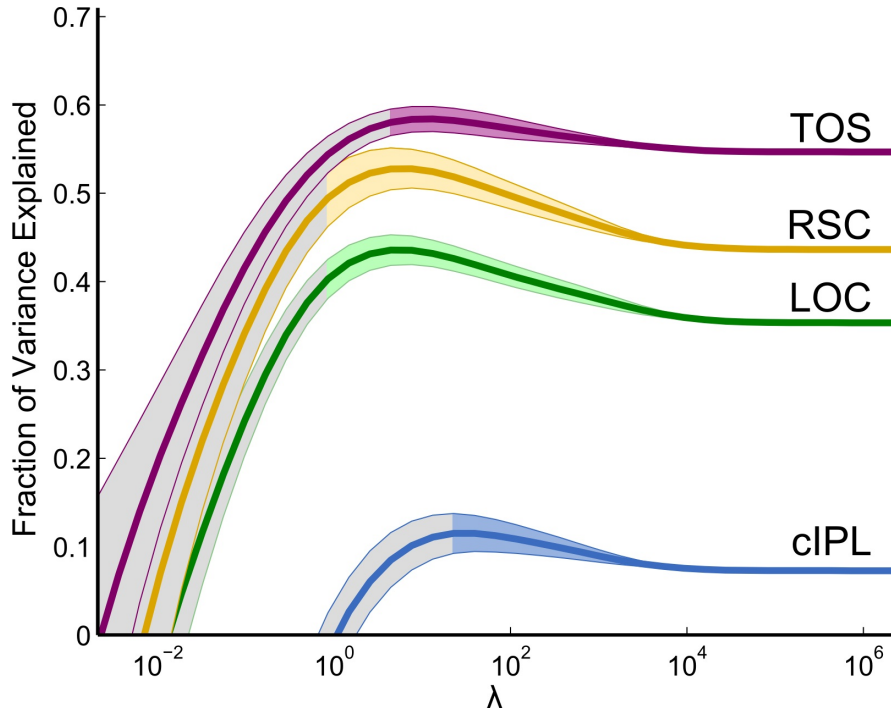
^b*Beckman Institute and Department of Psychology, University of Illinois at
Urbana-Champaign, Urbana, IL, USA*

*Corresponding author. Department of Computer Science, Stanford University, 353 Serra Mall, Stanford, CA 94305. Email address: chrisb33@cs.stanford.edu (C. Baldassano). Fax: +1 650 725 7411.



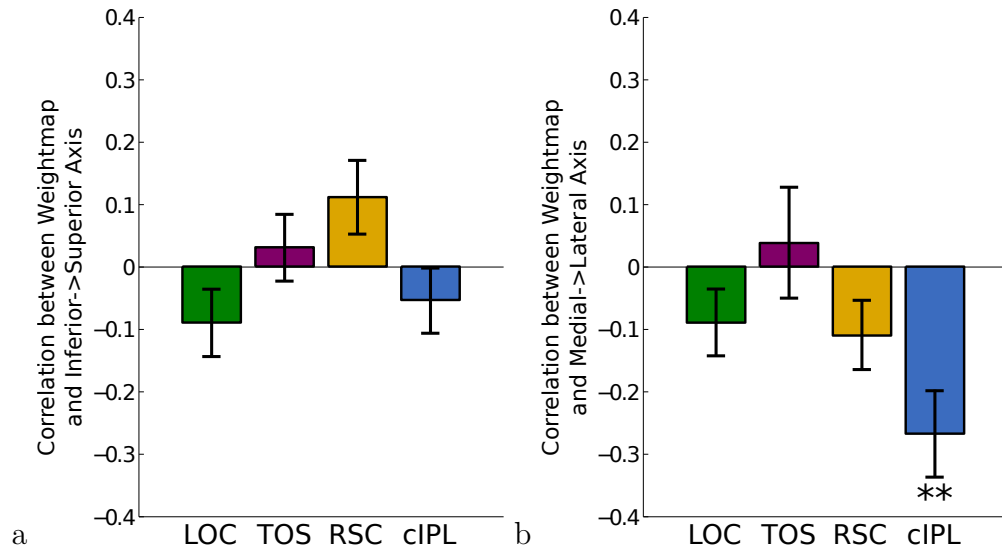
Supplementary Figure 1: Weightmaps Learned by Voxelwise Correlation

Rather than using our regularized connectivity approach, here the weight of each voxel for its connectivity with a seed ROI is simply set to the correlation between that voxel's timecourse and the seed ROI timecourse (contrast with main paper Fig. 2b). Although this approach can successfully detect that LOC and TOS are preferentially connected to posterior PPA, it fails to show significant effects for RSC and cIPL (LOC: $t_{17} = 6.02, p < 0.01$; TOS: $t_{17} = 7.03, p < 0.01$; RSC: $t_{17} = 0.22, p = 0.83$; cIPL: $t_{17} = -1.81, p = 0.09$; two-tailed t-test after z-transform). Error bars represent s.e.m. across subjects, ** $p < 0.01$.



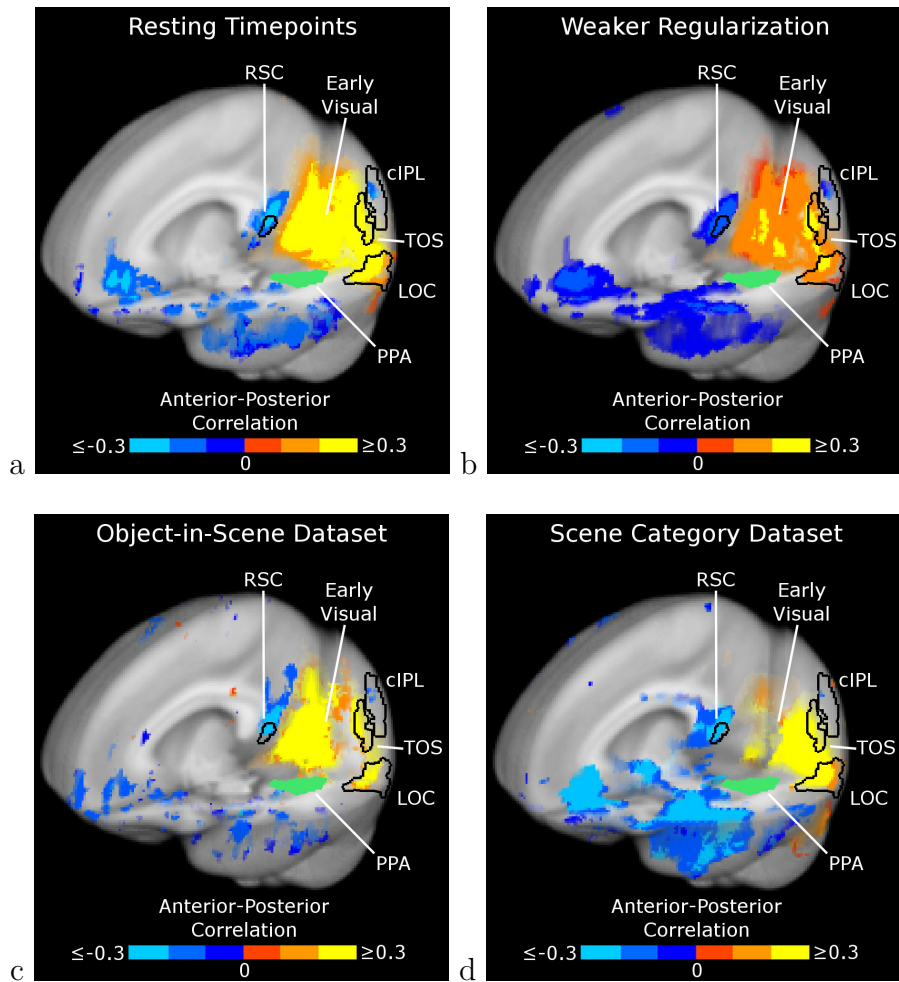
Supplementary Figure 2: Predictive performance of the connectivity model with varying regularization strength.

After learning a map of connectivity weights over PPA for each seed region (LOC, TOS, RSC, and cIPL) using one run, we measured how well the weighted average of PPA timecourses predicted the mean seed timecourse on the held-out runs. The X-axis (log scale) indicates the strength of spatial regularization applied; at the left side of the graph voxel weights are estimated independently, while the right endpoint corresponds to the traditional connectivity model in which only constant weight maps are learned. Intermediate regularization values (colored) produce better significantly generalization accuracy than those at the endpoints of the graph. This improvement occurs for a wide range of regularization strengths λ (LOC: $10^{-0.07} < \lambda < 10^{6.58}$; TOS: $10^{0.64} < \lambda < 10^{5.63}$; RSC: $10^{-0.07} < \lambda < 10^{6.34}$; cIPL: $10^{1.36} < \lambda < 10^{6.10}$; $t_{17} > 1.74, p < 0.05$ one-tailed t-test, uncorrected). The error bars indicate the standard deviation across subjects (controlling for performance as $\lambda \rightarrow \infty$).



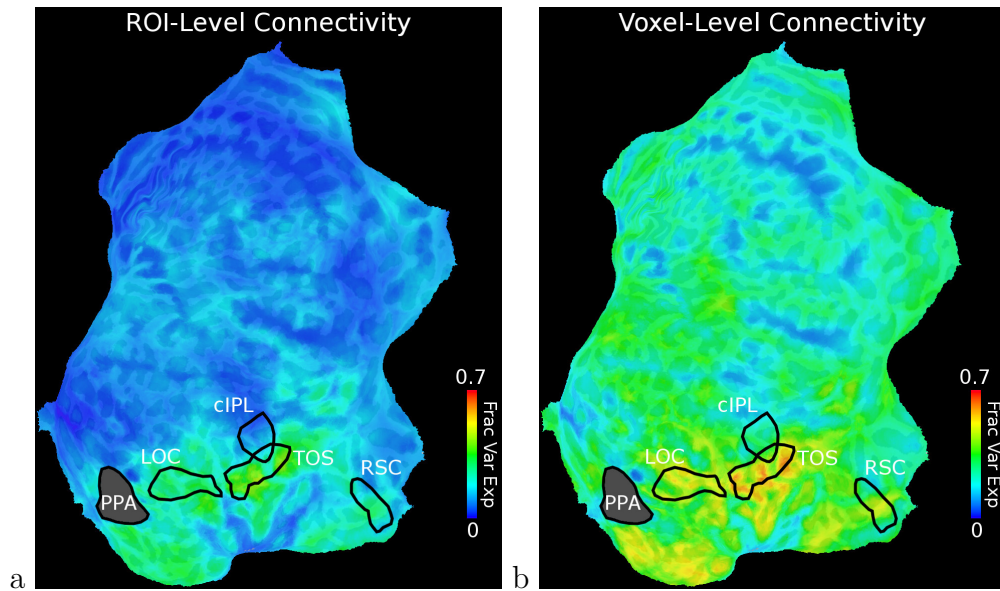
Supplementary Figure 3: Weightmap Correlations along Other PPA Axes

(a) The weightmaps for all areas show little correlation with the inferior to superior axis (LOC: $t_{17} = -1.71, p = 0.11$; TOS: $t_{17} = 0.63, p = 0.54$; RSC: $t_{17} = 1.87, p = 0.08$; cIPL: $t_{17} = -1.03, p = 0.32$; two-tailed t-test after z-transform). (b) Along the medial to lateral axis, cIPL is connected preferentially to the medial side of PPA, but other regions show no significant biases (LOC: $t_{17} = -1.73, p = 0.10$; TOS: $t_{17} = 0.55, p = 0.59$; RSC: $t_{17} = -1.95, p = 0.07$; cIPL: $t_{17} = -3.55, p < 0.01$; two-tailed t-test after z-transform). Error bars represent s.e.m. across subjects, ** $p < 0.01$.



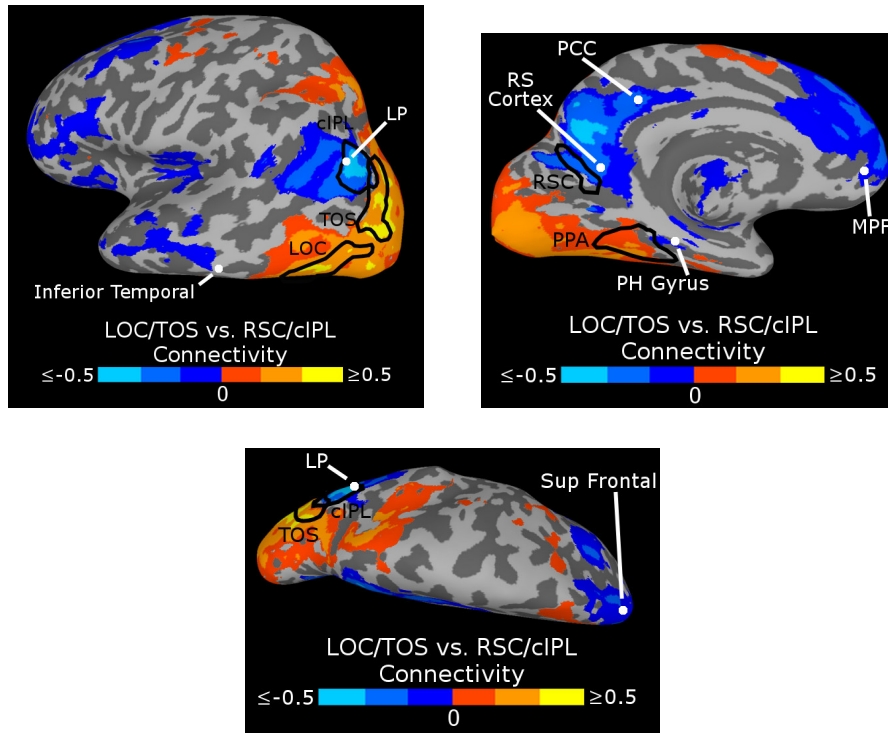
Supplementary Figure 4: Robustness of Connectivity Result to Task and Regularization Parameter.

(a) Using only “resting” timepoints between stimulus blocks yields similar results as when using all timepoints (FDR < 0.01, cluster size > 300mm³). (b) Rather than selecting an optimal regularization parameter using leave-one-run-in cross validation, we can optimize our regularization using leave-one-run-out cross validation, resulting in a smaller value of $\lambda = 0.54$. This does not change the overall pattern of connectivity (FDR < 0.01, cluster size > 300mm³). (c-d) Results for each set of subjects in the two experiments are similar to the whole-group results. These maps are thresholded at $p = 0.01$ (uncorrected) to show the trends in these smaller sample sizes.



Supplementary Figure 5: Fraction of Variance Explained in Searchlight Analysis.

The fraction of variance explained for each searchlight seed by PPA was calculated for both (a) the ROI-level method (using a spatially constant connectivity map over each PPA hemisphere, i.e. $\lambda \rightarrow \infty$) and (b) the voxel-level method. The fraction of variance explained by each voxel was computed as the average value of all searchlights including that voxel. Both methods show similar trends, with regions near LOC, TOS, and RSC having a large amount of shared variance with PPA, and other regions less related to PPA. The connectivity is substantially stronger overall for the voxel-level method, consistent with our results for the individual ROIs (main paper Fig. 2a).



Supplementary Figure 6: LOC/TOS vs. RSC/cIPL Connectivity

The data from Figure 6 is shown here across the entire inflated surface (FDR < 0.05, cluster size > 1000mm³). The Talairach coordinates of the cortical Default Mode Network (DMN) regions identified by Fox et al. (2005) are indicated with white dots. Voxels showing the same connectivity pattern as anterior PPA (RSC/cIPL connectivity greater than LOC/TOS connectivity) overlap closely with the DMN regions, showing that our RSC and cIPL regions are key components of this network.

Fox, M.D., Snyder, A.Z., Vincent, J.L., Corbetta, M., Van Essen, D.C., Raichle, M.E., 2005. The human brain is intrinsically organized into dynamic, anticorrelated functional networks. *Proc. Natl. Acad. Sci. U.S.A.* 102, 96739678.